Multiple states in the late Eocene ocean circulation

M.L.J. Baatsen[a,*], A.S. von der Heydt[a], M. Kliphuis[a], J. Viebahn[b], H.A. Dijkstra[a]

[a] Institute for Marine and Atmospheric Research Utrecht, Department of Physics and Astronomy, Utrecht University, Princetonplein 5, Utrecht 3584 CC, The Netherlands
[b] CWI, Amsterdam, The Netherlands

A B S T R A C T

The Eocene-Oligocene Transition (EOT) marks a major step within the Cenozoic climate in going from a greenhouse into an icehouse state, with the formation of a continental-scale Antarctic ice sheet. The roles of steadily decreasing CO_2 concentrations versus changes in ocean circulation at the EOT are still debated and the threshold for Antarctic glaciation is obscured by uncertainties in global geometry. Here, a detailed study of the late Eocene ocean circulation is carried out using an ocean general circulation model under two slightly different geography reconstructions of the middle-to-late Eocene (38 Ma). Using the same atmospheric forcing, both geographies give a profoundly different equilibrium ocean circulation state. The underlying reason for this sensitivity is the presence of multiple equilibria characterised by either North or South Pacific deep water formation. A possible shift from a southern towards a northern overturning circulation would result in significant changes in the global heat distribution and consequently make the Southern Hemisphere climate more susceptible for significant cooling and ice sheet formation on Antarctica.

1. Introduction

The climate during the Cenozoic era (last 65 million years, Myr) has changed dramatically from a warm, basically ice-free world to the present-day climate with large ice sheets in both polar regions. This long-term transition has not been smooth though: between slow trends of gradual warming or cooling several relatively rapid transitions have occurred, sometimes associated with a change in (quasi-periodic) variability on orbital time scales (Zachos et al., 2001a; Cramer et al., 2009).

Often the opening or closing of oceanic gateways is used in explanations of the sometimes rather dramatic climate shifts observed in the proxy record. For example, it has been suggested that the Northern Hemisphere glaciation in the Pliocene may have resulted from the establishment of the present-day Atlantic Ocean meridional overturning circulation after the closure of the Central American Seaway (Haug and Tiedemann, 1998). Similarly, the closure of the Indian-Atlantic Ocean connection through the Tethys seaway has been proposed to have had profound impacts on the Miocene climate (Harzhauser et al., 2007). However, the most widely discussed example of a gateway-related cause for climate change is the hypothesis that the establishment of the Antarctic Circumpolar Current due to opening of the Southern Ocean gateways has thermally isolated Antarctica such that a large ice sheet could appear at the Eocene-Oligocene boundary (Kennett, 1977). While

all of these hypotheses are being debated for various reasons (e.g. Antarctic glaciation forced by declining CO_2 levels (Gasson et al., 2014) rather than ocean gateways), often it is the uncertainty in timing and precise occurrence of the gateway closure/opening that makes a direct causal relationship with a climate transition problematic.

Uncertainty in paleobathymetry arises because of the complicated structure of plate boundaries and continents meeting each other. However, there are also more subtle uncertainties in geographical boundary conditions such as the positioning of plates (and continents) with respect to each other, which is only at the beginning of being quantified (Torsvik et al., 2012; van Hinsbergen et al., 2015). Plate-tectonic models rely on a specific frame of reference to determine how the plates are positioned with respect to the Earth's mantle (Dupont-Nivet et al., 2008). Currently, two such frameworks are used, one referred to as HotSpot (HS, Seton et al. (2012)) and the other as PaleoMag (PM, Torsvik et al. (2012)). Global middle-to-late Eocene reconstructions were made in these two different frames of reference (Baatsen et al., 2016) for use as boundary conditions for ocean-climate models. While the gateway regions are exactly the same in both versions, the rotation of the poles in the PM frame of reference results in continents shifted or rotated by as much as 5–6° with respect to the HS one.

As more and more time slices of paleogeography become available and are being used for ocean and climate model studies (von der Heydt and Dijkstra, 2006; Haywood et al., 2011; Herold et al., 2014; Lunt

* Corresponding author.
E-mail addresses: m.l.j.baatsen@uu.nl (M.L.J. Baatsen), a.s.vonderheydt@uu.nl (A.S. von der Heydt), m.kliphuis@uu.nl (M. Kliphuis), j.viebahn@cwi.nl (J. Viebahn), h.a.dijkstra@uu.nl (H.A. Dijkstra).

et al., 2016), we consider it important to determine how the modelled global ocean circulation is dependent on the chosen boundary conditions. In this paper, we study the sensitivity of the ocean circulation to relatively moderate changes in continental geography (Baatsen et al., 2016) using a global ocean-only model for the middle-to-late Eocene. We find an unexpected sensitivity of the Eocene global ocean flow to paleobathymetry and explain this by the occurrence of multiple equilibria.

2. Methods

2.1. Ocean model

The global version of the Parallel Ocean Program (POP v2.1) model (Smith et al., 2010) is used for computing the circulation in both (HS and PM) paleobathymetries. Horizontal viscosity is anisotropic (Smith and Mcwilliams, 2003) and horizontal tracer diffusion follows the parameterisation of Gent and Mcwilliams (1990). The model uses the KPP-scheme for vertical mixing coefficients (Large et al., 1994). The model is set up with a nominal 1° horizontal resolution (320×384 grid points) and 60 vertical (non-equidistant) layers using a curvilinear projection. We use the bipolar grid version of POP with the southern pole situated at 90°S in the Antarctic continent, and the northern pole is relocated to Greenland (at 68°N, 20°W). A simple sea ice module is enabled that introduces sea ice whenever the sea surface temperature drops below $-1.8°$ C.

A global geography reconstruction made for 38 Ma, using the method described in Baatsen et al. (2016), is shown in Fig. 1 in a curvilinear projection as used by the ocean model here. This reconstruction uses the Torsvik et al. (2012) PaleoMag reference frame, the Müller et al. (2008) ocean bathymetry and the Wilson et al. (2012) Antarctic topography. White contour lines in Fig. 1 indicate the changes

in the positions of the continents with respect to the PM reconstruction, when using a HS reference frame as in Seton et al. (2012).

2.2. Model forcing

The atmospheric forcing is taken from a lower resolution (T42; ~ 2.5°) Eocene coupled climate model (CCSM3) simulation under $4 \times$ pre-industrial CO_2 (i.e. 1120 ppm) (Huber and Caballero, 2011). Surface fields of wind stress, freshwater flux, heat flux and sea surface temperature from CCSM3 are adjusted to the new model grid as shown in Fig. 2. Monthly climatologies (using a 50-year average) are considered, from which original land masses are removed using natural neighbour interpolation. Next, surface forcing fields are adjusted to the new land-ocean mask and interpolated onto the curvilinear grid. Localised extremes from river runoff in surface fresh water fluxes (Fig. 2a) are removed and global fields are bias corrected to conserve the global salt budget. Larger scale effects from run-off, precipitation and evaporation are still present in the adjusted forcing as seen in Fig. 2b. Similarly, a bias correction is applied to the surface heat fluxes to conserve the global heat budget at the atmosphere-ocean interface. The ocean model is then forced by the adjusted surface fresh water flux, wind stress (shown in Fig. 9) and heat flux, where the latter is combined with restoring conditions to sea surface temperatures.

Three different simulations are carried out; the first using a PaleoMag geography (referred to as ' PM'), the second using a HotSpot geography (' HS') and the third starting from the Paleomag configuration but using adjusted surface fresh water fluxes (PM Adjusted). The PM Adjusted case serves to test the stability of the overturning regime by perturbing the system for a limited amount of time through adding 1Sv of integrated fresh water flux to the South Pacific and doing the opposite in the North Pacific (blue and red boxes in Fig. 2a, respectively).
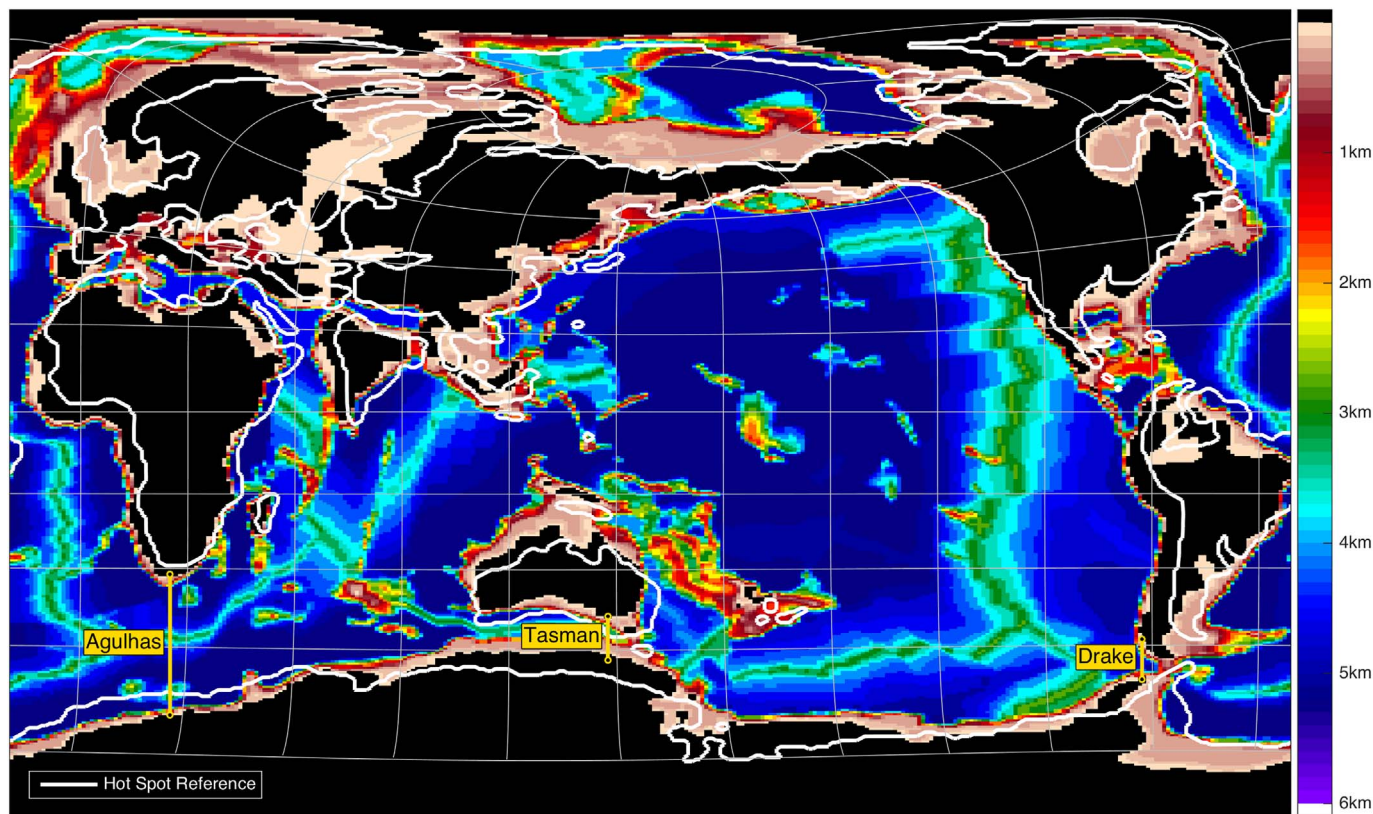

Fig. 1. Global bathymetry grid in curvilinear projection as used by the model; black shading shows the land mask and colours indicate depth. The model grid is based on a PaleoMag (PM) referenced 38 Ma reconstruction, while the white contour line indicates the shorelines using a HotSpot (HS) framework. A rectangular projection grid is added in grey, featuring 30° intervals in longitude and 20° in latitude. Thick yellow lines denote the positions of three Southern Ocean transects with their respective names, which will be used in the text below.
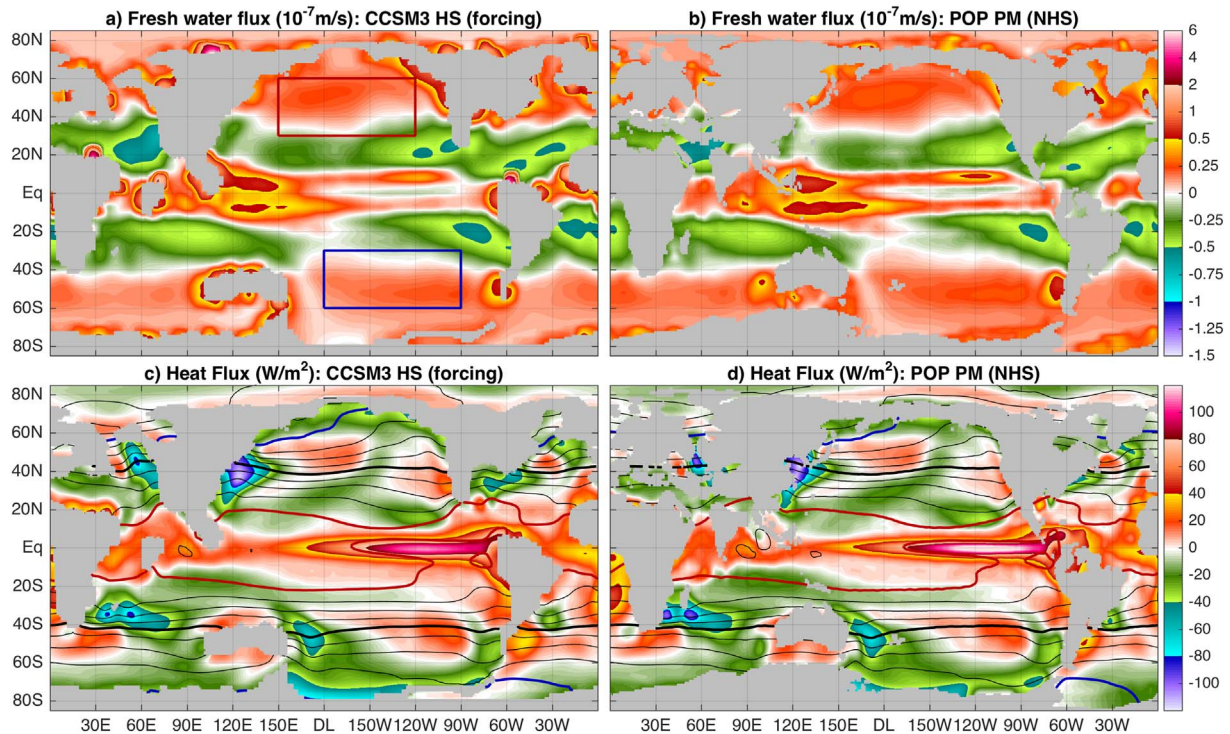
Fig. 2. Surface fresh water flux from **a)** the CCSM3 forcing and **b)** adjusted to the PaleoMag geography as used in the ocean-only simulations. Red and blue rectangles denote the areas of changed fresh water fluxes for the adjusted PaleoMag simulation in the North and South Pacific, respectively. Surface heat flux (shading) and sea surface temperatures (contours every 2.5°C; blue: 10°C, black: 20°C and red: 30°C), again from the **c)** CCSM3 forcing and **d)** adjusted to the PaleoMag geography.

2.3. Model spin-up

The ocean state is initialised for both PM and HS cases as motionless and having a horizontally homogeneous temperature distribution, decreasing linearly (as a function of model levels) from 15°C at the upper level down to 9°C at the bottom. Model simulations are carried out over 3200 and 2500 years towards an equilibrium state for the PM and HS cases, respectively. In the PM Adjusted case, the initial state is that of the PM case at model year 3000 after which the adjusted forcing is applied for 200 years. The model is then run for another 800 years with the unperturbed forcing (i.e. identical to that of the PM case) resulting in a total of 1000 model years. Trends of (Global, Pacific and Atlantic) average temperature and salinity are shown in Fig. 3 for the upper 1000 m, below 2000 m and full depth. An overview of the drifts in temperature and salinity for all three simulations is given in Table 1. Upper 1000 m temperatures equilibrate well and show little to no drifts in the last 500 years of each simulation (200 for PM Adjusted). Deep ocean temperatures take longer to settle, especially in the PM case which requires a longer spin-up time. Drifts in global mean temperature are generally in the order of 1 K per 10^4 years over the last 200 model years. Globally averaged salinity continues to show a minor drift of a few psu per 10^5 years and is rather steady throughout the spin-up. Despite the surface budget being closed, there is still a small drift in the global salt budget due to numerical errors but this is not problematic (a ~0.1 psu increase is seen through the entire run).

To monitor the development of the flow, several indicators are used as described below. Three meridional transects are considered from west to east, named Agulhas, Tasman and Drake (as shown in Fig. 1) and connecting Africa, Australia and South America to Antarctica, respectively. The volume transport (in Sv) through these three transects is displayed as solid curves in Fig. 4a. The transient behaviour shows the importance of a long model spin-up (beyond 2000 years) as there are still substantial changes around model year 1500 (PM) and 1000 (HS). The abrupt changes in volume transports can be linked to an invigoration of the meridional overturning circulation (MOC), shown in

Fig. 4b. Time series of global MOC strength are shown for both hemispheres, where black indicates the maximum value of the northern overturning cell while red does so for the (minimum of the) southern cell. The effects of enhanced overturning are also visible in average temperature and salinity in Fig. 3. Temperatures below 2000 m are seen to increase first due to thermal diffusion of surface warmth, after which more efficient ventilation cools down the deep ocean again for the PM case. A steady warming of oceanic bottom waters acts to reduce thermal stratification in the initial phases of spin-up (1000–1500 years); the stratification becomes sufficiently small at some point to allow for transition towards a flow regime with significantly stronger meridional overturning.

3. Results

3.1. Geometry-dependent flow patterns

Despite the minor differences between the HotSpot and PaleoMag geometries, they result in profoundly different (equilibrium) flow regimes (comparing dotted (HS) to solid (PM) curves in Fig. 4). In the following we discuss the resulting flow pattern averaged over the last 50 years of simulation. In the PM case, relatively large zonal transports through Southern Ocean transects are associated with a strong Southern Ocean sourced meridional overturning circulation. The opposite is seen in the HS simulations, where the Southern Ocean zonal transports and the southern overturning circulation are relatively weak, while the northern overturning circulation is about as strong as the southern overturning in the PM case.

The equilibrium state sea surface temperature (SST), sea surface salinity, barotropic streamfunction and sea surface height (SSH) for the PM simulation are shown in Fig. 5a,c. The main feature of the global circulation is an expansive Indo-Pacific subtropical gyre system spanning 3/4 of the tropics. The associated warm pool with annual mean SSTs reaching almost 35°C, covers most of the Indian Ocean and is accompanied by an extended cold tongue to its East. The sub-polar
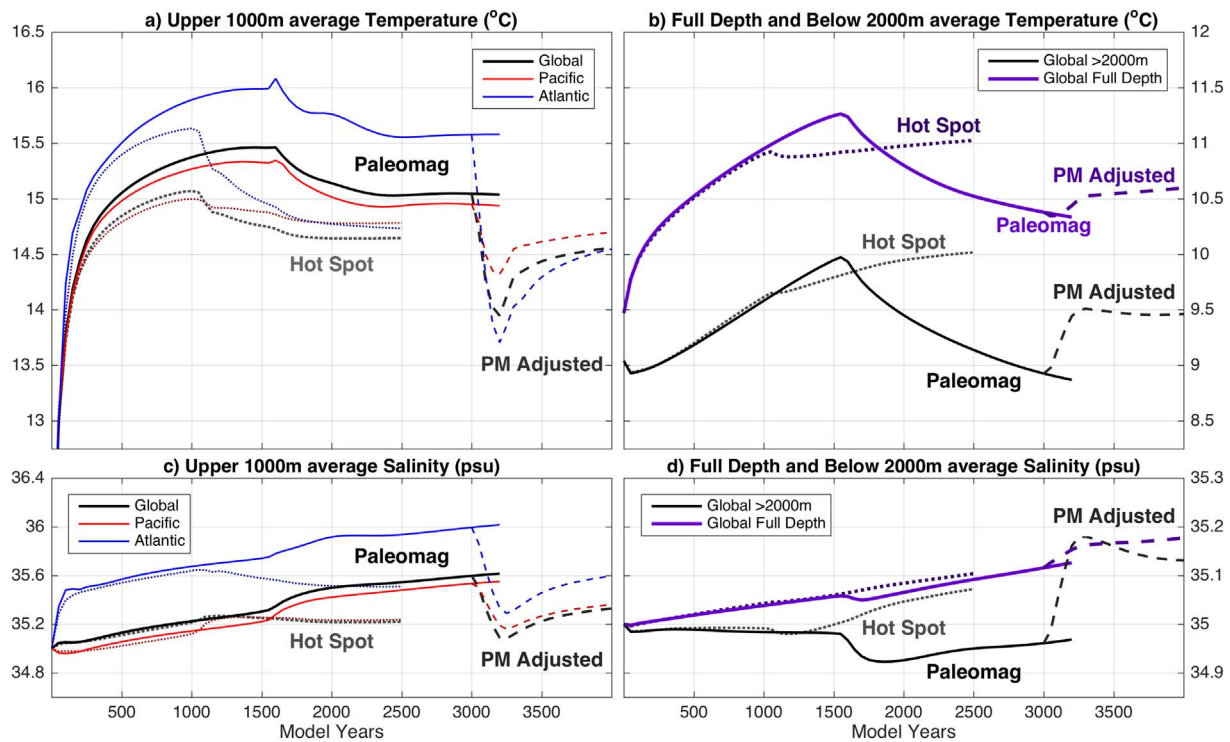
Fig. 3. Time series of average temperature for **a)** upper 1000 m and **b)** full depth (purple) and below 2000 m (black). Upper 1000 m averages are separated in global (black), Pacific-only (red) and Atlantic-only (blue) means, showing the entire spin-up of the PaleoMag (solid), HotSpot (dotted) and adjusted PaleoMag (PM Adjusted; dashed) simulations. **c)** and **d)** as in a and b but for time series of average salinity.

Table 1
Overview of all three POP spin-up simulations with their boundary conditions, spin-up time and drifts in global mean temperature and salinity over the last 200 model years. Forcing subscripts denote adjustment to geography and 'SFWF' indicates changed surface fresh water flux. Normalised drifts $\Delta T/T$ and $\Delta S/S$, with T temperature in Kelvin and S salinity in psu, are also shown for each case using the same period.

Simulation	PM	HS	PM Adjusted
Geography	38 Ma Paleomag	38Ma HotSpot	38Ma Paleomag
Spin-up (years)	3200	2500	1000
Forcing	$CCSM3_{PM}$	$CCSM3_{HS}$	$CCSM3_{PM}$ SFWF
ΔT (K/year)	$-2.2 \cdot 10^{-4}$	$8.8 \cdot 10^{-5}$	$1.1 \cdot 10^{-4}$
ΔS (psu/year)	$5.2 \cdot 10^{-5}$	$4.0 \cdot 10^{-5}$	$2.8 \cdot 10^{-5}$
$\Delta T/T$ (/year)	$-7.7 \cdot 10^{-7}$	$3.1 \cdot 10^{-7}$	$3.8 \cdot 10^{-7}$
$\Delta S/S$ (/year)	$1.5 \cdot 10^{-6}$	$1.1 \cdot 10^{-6}$	$8.1 \cdot 10^{-7}$

regions are mild at 10–20° C and reflect a climate with high greenhouse gas concentrations and a reduced equator to pole temperature gradient. Because of its relatively isolated configuration, the Arctic is significantly colder than the Southern Ocean. However, temperatures hardly go below freezing and sea ice only occurs sporadically and very locally. The SSH pattern denotes pronounced gyre circulations across most of the high latitudes (beyond 45°N/S) and a strong zonal current at the wind stress maximum around 45°S. SSH fields further suggest the presence of at least a shallow circumpolar flow in the Southern Hemisphere, although the Southern Ocean passages are strongly limited in depth and width. As shown in Fig. 4a, volume transport through the Drake Passage is only about 15 Sv in the PM case and 5 Sv in the HS one.

The equilibrium state for the HS case accordingly shows warmer and more saline North Pacific high latitude regions (Fig. 5b,d) compared to the PM case, while the opposite holds for the South Pacific. Apart from the Tasmanian Gateway, volume transport through the Southern Ocean passages drops to very low values indicative of a circulation dominated by gyres in the Southern Hemisphere. The differences between PM and HS cases thus mostly result from reversed

patterns in MOC, where the HS geometry favours Northern and the PM geography favours Southern Hemispheric deep water formation. Patterns of mixed layer depth and basin-specific overturning stream functions (not shown) indeed confirm that all of this deep water formation occurs in the South versus North Pacific Ocean for the PM and HS case, respectively.

3.2. Multiple equilibria within the Paleomag geography

Recalling that both PM and HS simulations use essentially the same atmospheric forcing conditions, this result suggests a strong dependence of the circulation pattern on the model geography. To investigate the occurrence of multiple equilibria in the overturning state, we performed an additional simulation using a density perturbation (PM Adjusted). Starting from the ocean state of the PM simulation at model year 3000, a negative freshwater flux (−1 Sv) is added to the sub-polar North Pacific. Similarly, a +1 Sv forcing is applied to the sub-polar South Pacific region as shown in Fig. 2a. The total flux of 1 Sv is divided over a 30°× 90° area and results in an anomalous forcing of ~ 0.5 · 10^{-7}m/s, which is in the same order of magnitude as the unperturbed fresh water fluxes. To let the circulation adjust to these density perturbations, anomalous freshwater fluxes are applied for 200 years. Afterwards, the simulation is continued under the original forcing for another 800 years to reach equilibrium again (see dashed lines in Fig. 3). This makes the third simulation spin-up significantly shorter compared to those of the PM and HS case, but it did not start from a motionless state with a generalised temperature and salt distribution. Model drifts after 1000 years for the PM Adjusted case shown in Table 1 are of the same order as those seen in the other simulations. Additionally, the density perturbation drives an enhanced meridional overturning circulation for 200 years which effectively mixes the deep ocean more quickly and speeds up the equilibration.

Indicators of the transient flow are again shown in Fig. 4, with the dashed curves representing the PM Adjusted case. The density perturbation inverts the meridional overturning circulation (Fig. 4b). After an
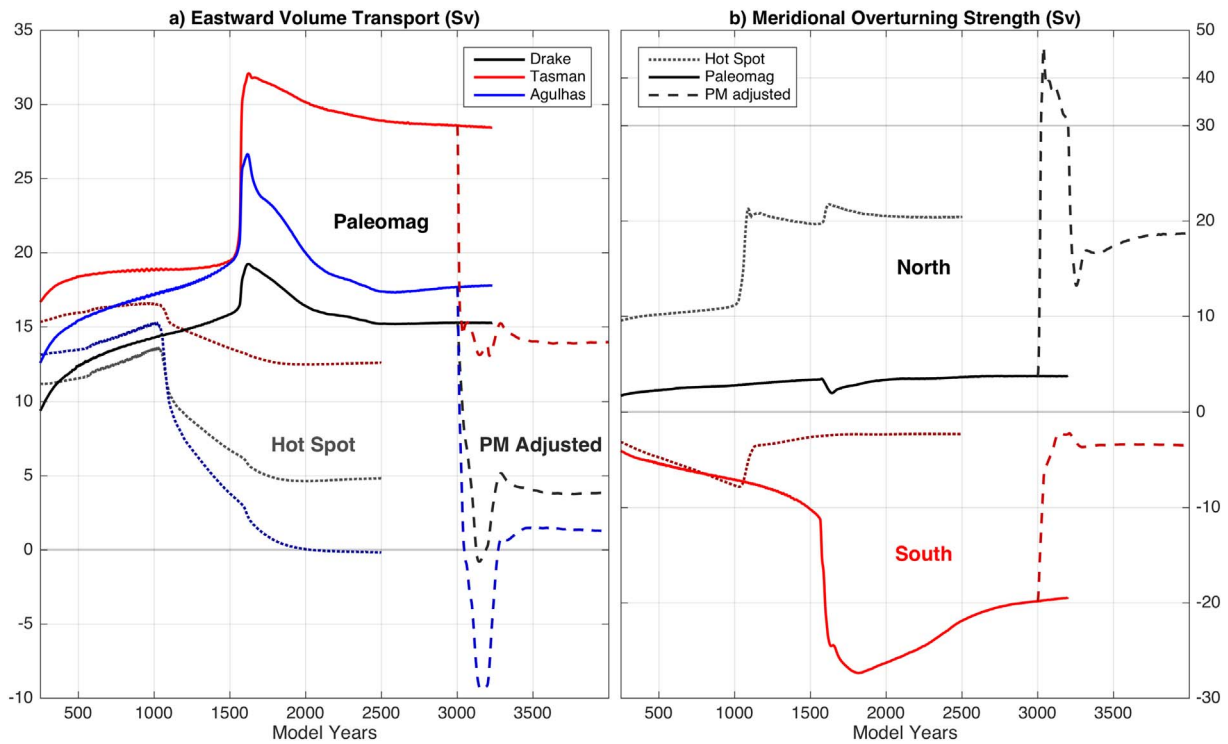
Fig. 4. **a)** Integrated volume transport through the Agulhas transect (blue), Tasmanian Gateway (red) and Drake Passage (black). Yearly averaged values are shown for all three simulations starting at model year 250: case PM (solid), HS (dotted) and PM2 (dashed). **b)** As in a) for the maximum global meridional overturning strength in the Northern (black) and Southern (red) Hemisphere.

overshoot (caused by the altered forcing), the transports settle to values similar to those seen in the HS case (with North Pacific deep water formation). In the PM Adjusted equilibrium state, the maximum of the meridional overturning stream function (dashed curves in Fig. 4b) clearly demonstrates the dominant northern sinking. The results of the

PM Adjusted simulation thus effectively show that different overturning states can be realised in the PaleoMag referenced geography under the same atmospheric forcing. The relatively large flow through the Tasmanian Gateway in the PM case compared to PM Adjusted (and HS) suggests that this gateway transport is not correlated with a deep
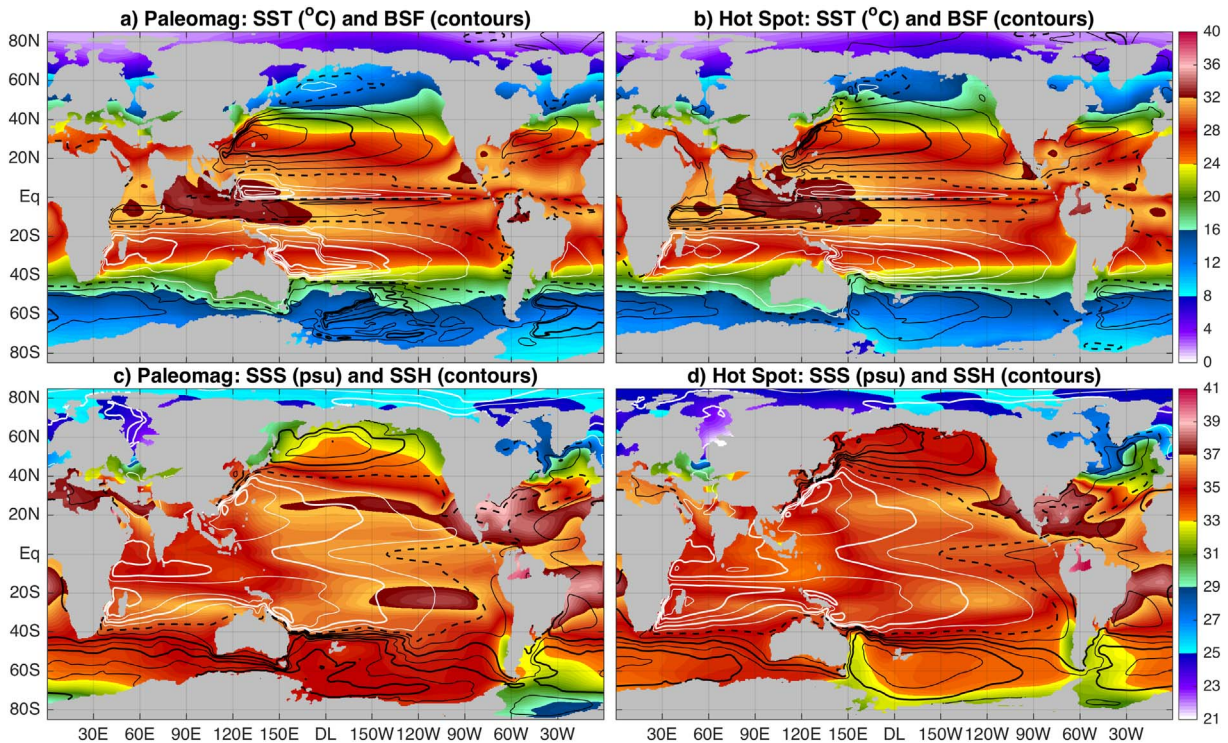

Fig. 5. Sea surface temperatures (SST; shading) and barotropic stream function (BSF; contours every 10 Sv; white: positive, black: negative, dashed line at 0) for **a)** the PM and **b)** the HS case. PM Sea surface salinity (SSS; shading) and sea surface height (SSH; contours every 15 cm; white: positive, black: negative, dashed line at 0) for **c)** PM and **d)** HS, respectively.
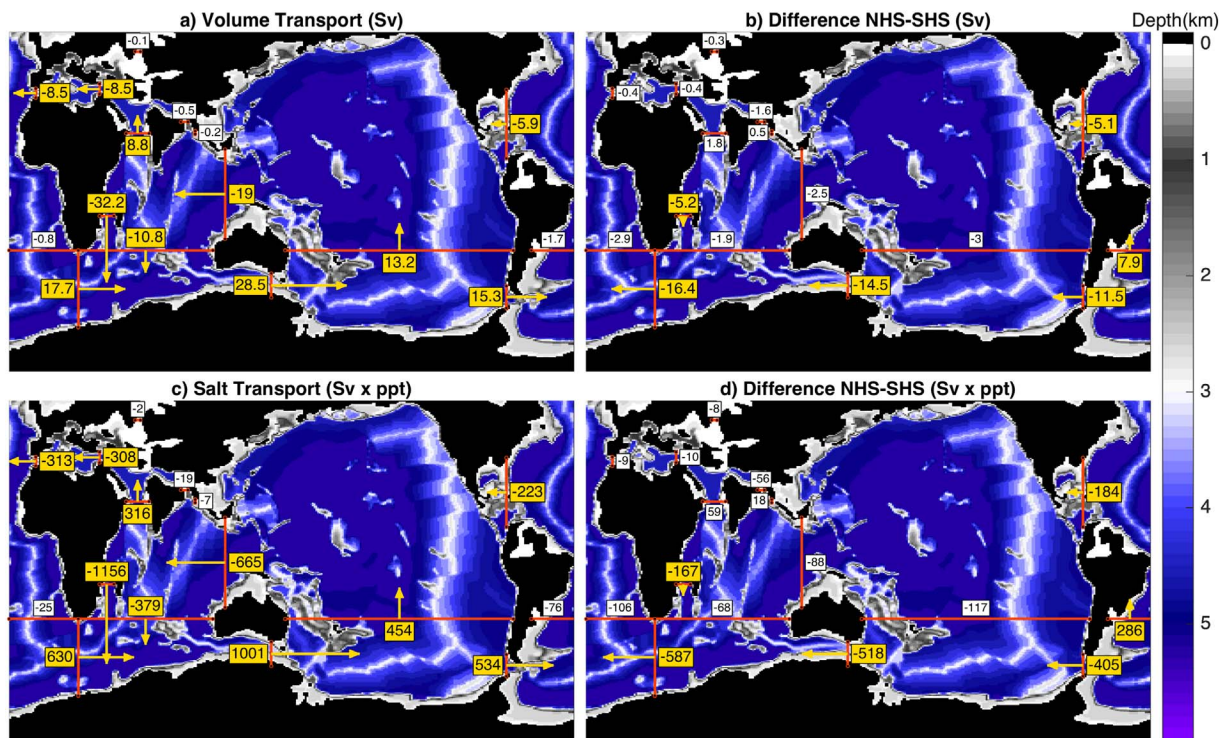
Fig. 6. a) Volume transports for the SHS equilibrium state. **b)** Difference fields (NHS-SHS) of the volume transports. **c)** and **d)** same as a) and b) but for the total salt flux. Boxes and arrows show the magnitude and direction of the largest and most important fluxes and flux differences, with gold coloured ones highlighting the largest and most important values. Transports are perpendicular to the transects, where positive values denote either northward or eastward flows. Background shading indicates model grid depth and red lines show the transects at which transports are calculated.

circumpolar flow. Other Southern Ocean passages never show such large flows and thus the difference can best be explained by geostrophic adjustment to an enhanced meridional density gradient. Deep water formation and the associated salt advection feedback act to increase the density at high latitudes and thus the density gradient. For clarity, the different equilibrium states found within the PaleoMag geography will be referred to as SHS (southern hemisphere sinking; PM) and NHS (northern hemisphere sinking; PM Adjusted) onwards, reflecting their crucial difference in overturning state.

A more detailed view on the SHS state and the differences (NHS-SHS) between both states considering both global volume, heat and salt transports (shown in Fig. 6) reveals that transport values in the Southern Ocean are generally small compared to the present day. This corresponds to an ocean state dominated by gyre circulations in which flows through gateways are small, or are compensated for within larger transects. A circumpolar current of 15–20 Sv is present in the Southern Ocean, limited mostly by the Drake Passage (because of its high southerly latitude). The largest transport is seen in the Mozambique channel, characterising the western intensification of the South Indian subtropical gyre and the origin of the Agulhas current. In addition, there seems to be a net 10–15 Sv anticyclonic flow around Australia in response to the density gradient in the South Pacific. Finally, a 5–10 Sv global westward current is present in the tropics, allowed by the Neo-Tethyan passages and through Central America. Salt fluxes show a similar picture, closely related to the main currents. What stands out is the large amount of salt transported eastward through the Tasmanian Gateway. A net southward flux in the South Indian Ocean injects additional salt eastward into the South Pacific sub-polar gyre, helping to increase the density and thus the deep water formation. Since the Tasmanian Gateway is at a higher latitude in the HS reconstruction it is significantly harder to force high salinity water through this gateway, and into the sub-polar South Pacific. As a result, enhanced salt transport seems to be the reason why the PM configuration favours Southern Hemispheric sinking, while the HS one does not. When the overturning

is reversed (NHS state), Southern Ocean transports dramatically decrease and a circumpolar current ceases to exist. Westward flow through Central America is now enhanced as a result of a stronger gyre circulation in the North Pacific.

Patterns of the different equilibrium global MOC states (SHS and NHS) are presented in Fig. 7a–b, clearly showing the different sinking patterns. In addition to the meridional overturning stream function, trajectories are calculated for several parcels starting (for each case) in the areas of deep water formation and assuming that they follow the zonally integrated flow (also in Fig. 7 a–b). This assumption is based on the observation that no deep sinking occurs outside of the Pacific Ocean. While both overturning cells are similar in extent and strength (apart from being mirrored), the NHS one appears to be shallower (related to differences in bathymetry and density between source regions). Weaker flow below 2 km depth results in water parcels taking almost twice as long (600–800 years in NHS instead of ~400 years for SHS) to reach the equator at a depth of 4 km. These values are purely indicative, but suggest that bottom water masses in the equatorial Pacific can have very different characteristics besides those determined by their source regions. Such a change towards an older water mass would cause a significant reduction in the solubility of carbonate and thus a decrease in the carbonate compensation depth (CCD). An example of such a sharp reduction in solubility is observed at site ODP1218 in the Equatorial Pacific (Coxall et al., 2005) as a dissolution event right before the first step of the EOT.

Zonally integrated meridional heat transports (Fig. 7c) show a picture in agreement with a switch between overturning regimes. The NHS state heat transport looks similar to that of the present day, where the North Pacific takes over the contribution of the North Atlantic with a maximum northward heat transport of about 2 PW in the subtropical gyre. In the SHS case, an overall amount of 0.5 –1 PW is redistributed from the Northern towards the Southern Hemisphere. The overturning cell mostly serves to push oceanic heat beyond 45° latitude, significantly warming the high latitude regions where deep sinking occurs.
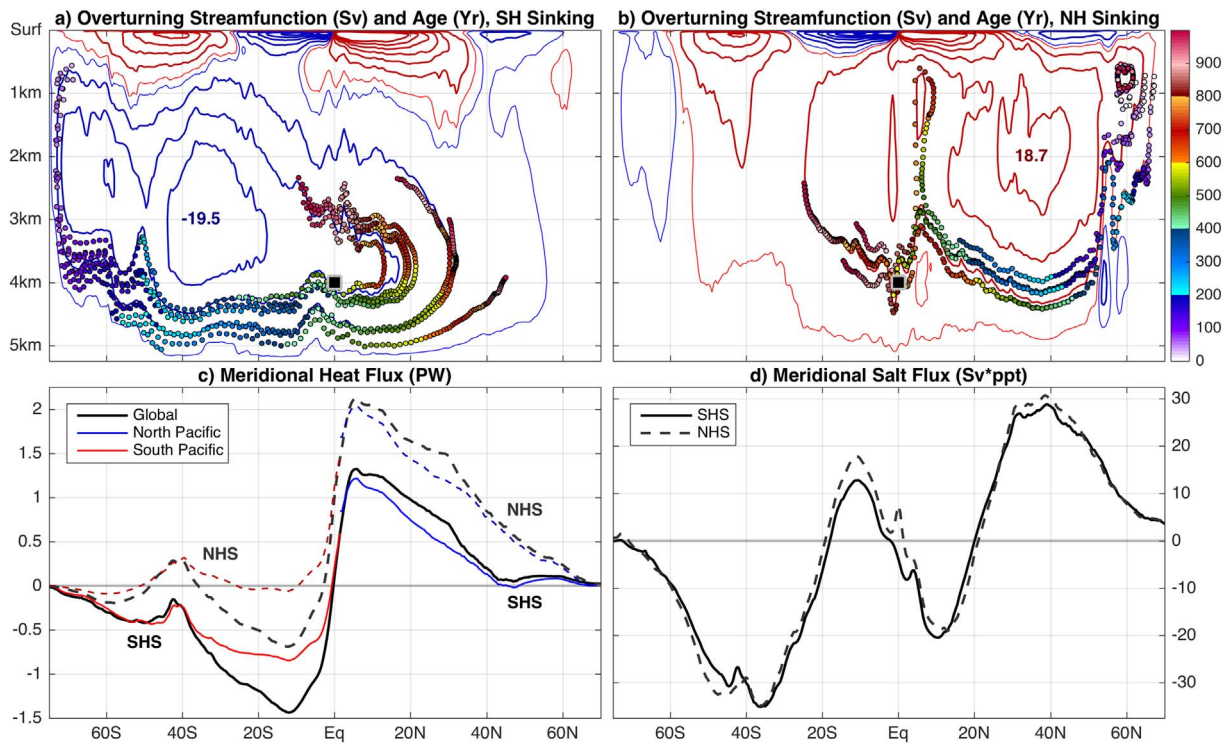
Fig. 7. Global meridional overturning stream function for the **a)** SHS (PM) and **b)** NHS (PM Adjusted) case, with contours drawn every 5 Sv (red: positive, blue: negative, thin lines at $+/-1$ Sv) and numbers indicating maximum values. Coloured dots show different parcel tracks and 'age' (in years) and the black square denotes the paleo location of site ODP1218. **c)** Global meridional heat transport in the SHS (solid) and NHS (dashed) state, coloured lines show the contribution of the North (blue) and South (red) Pacific Ocean. **d)** As in c), but for meridional salt transports.

Looking at the contribution of only the Pacific Ocean (red and blue), both the total heat fluxes and differences between overturning states are dominated by this basin. Finally, zonally integrated meridional salt transports (Fig. 7d) show a typical pattern where salt is advected away from evaporative regions in the subtropical gyres towards both the tropics and higher latitudes. Changes between SHS and NHS states are minimal here and probably limited by fixed surface fresh water fluxes and the implied meridional response in the model. This is different for the meridional heat transport, where mixed (considering both heat fluxes and SSTs) boundary restoring conditions are used.

Temperature and salinity differences (NHS-SHS) between both states are shown in Fig. 8 at the surface (a), below 2 km depth (b) and for a zonally averaged Pacific cross section (c and d). When switching from the SHS towards the NHS state, a general warming and salinification of North Pacific surface waters occur at the expense of cooling and freshening in the South Pacific. These changes are more localised and intense in the north, while they are more evenly distributed across the South Pacific sub-polar gyre. Furthermore, the associated density changes are shallower thus having a limited effect on stratification across southern high latitudes. Additionally, the Atlantic and Indian parts of the Southern Ocean become warmer and more saline in response to a vanishing proto-circumpolar current. Vertical cross sections (Fig. 8 c–d) indicate a general warming of the deep ocean, related to changes in the deep water formation source region. A tongue of colder and fresher water in the NHS state finally suggests the presence of a South Pacific intermediate water mass, similar to the one seen in the present-day South Atlantic Ocean. The largest changes in temperature are seen below the surface as an effect of the mixed restoring conditions including SST. This is in contrast to salinity changes that are maximised at the surface, where only fresh water fluxes are considered. The salt advection feedback, stabilising the overturning regime, is thus facilitated by the surface boundary conditions applied here.

A comparison of wind stress curl and barotropic stream function fields of the original CCSM3 simulation (from which the atmospheric

forcing was derived) with those of the HS and PM (both SHS and NHS) cases is made in Fig. 9. POP model results (Fig. 9 b–d) are interpolated on a 1° × 1° and smoothed using a 3° × 3° mask to be comparable to the CCSM3 fields (Fig. 9a). Forcing by the wind is similar for all cases, with only minor shifts and adjustments to the changing continental configuration. As a result, depth averaged flow patterns are also similar and show little change between the HS and PM case when only looking at northern sinking solutions (Figs. 9 b and d). More significant changes in gyre strength can be seen in the Indian Ocean, related to the different position of India compared to the one used in the CCSM3 simulation (forcing). Enhanced Southern Ocean zonal flow, stronger South Pacific and weaker North Pacific gyres are present in the SHS case as compared to both NHS cases (HS and PM) and the CCSM3 simulation. Despite featuring a southern sinking state as in the PM case (c; SHS), the CCSM barotropic stream function resembles that of the HS (b; NHS) solution more closely. This resemblance is likely the combined effect of a better matching model geography (CCSM geography and HS use the same frame of reference) and the coarser resolution that obscures the effects of bathymetry on the depth-averaged flow (mainly South Pacific).

Differences in barotropic stream function between the NHS and SHS states are similar to those between the HS and PM cases (contours in Fig. 10). Therefore, changes in flow pattern are dominated by a shift in sinking regime as opposed to the model geography. Some more subtle flow changes related to differences in geography are still present, mainly caused by changes in western boundary currents (e.g. Mozambique Channel and East Australian Current) or the positioning of gateways (e.g. South Atlantic east of the Drake Passage). For this specific case, changes in model geography are thus a significant influence on the preferred overturning state, but do not change the associated depth-averaged circulation dramatically.

The estimated $\delta^{18}O$ signal, based on a simple parameterisation using salinity and temperature (Broecker, 1989), due to a switch from the SHS into the NHS state is shown in Fig. 11. Changes in the mixed layer reflect straightforward shifts in temperature and salinity in the different
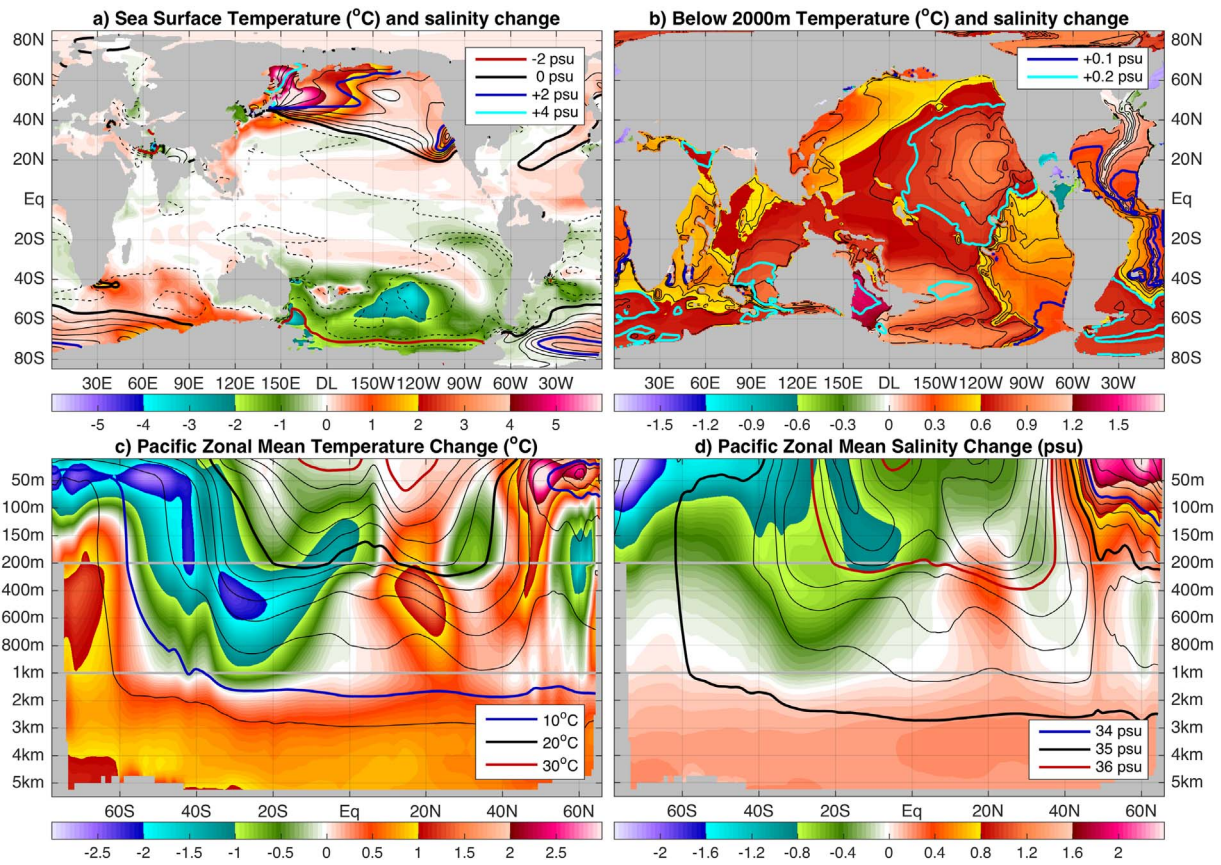
Fig. 8. a) NHS-SHS state sea surface temperature (shading) and salinity (contours every 0.4 psu) change, **b)** similar for changes below 2000 m depth with contours every $2 \cdot 10^{-2}$ psu. **c)** Pacific zonal mean temperature change (NHS-SHS) and SHS temperature (contours every 2°C). Vertical scaling changes at 200 m and 1 km depth. **d)** as in c for salinity change and SHS salinity (contours every 0.25 psu).
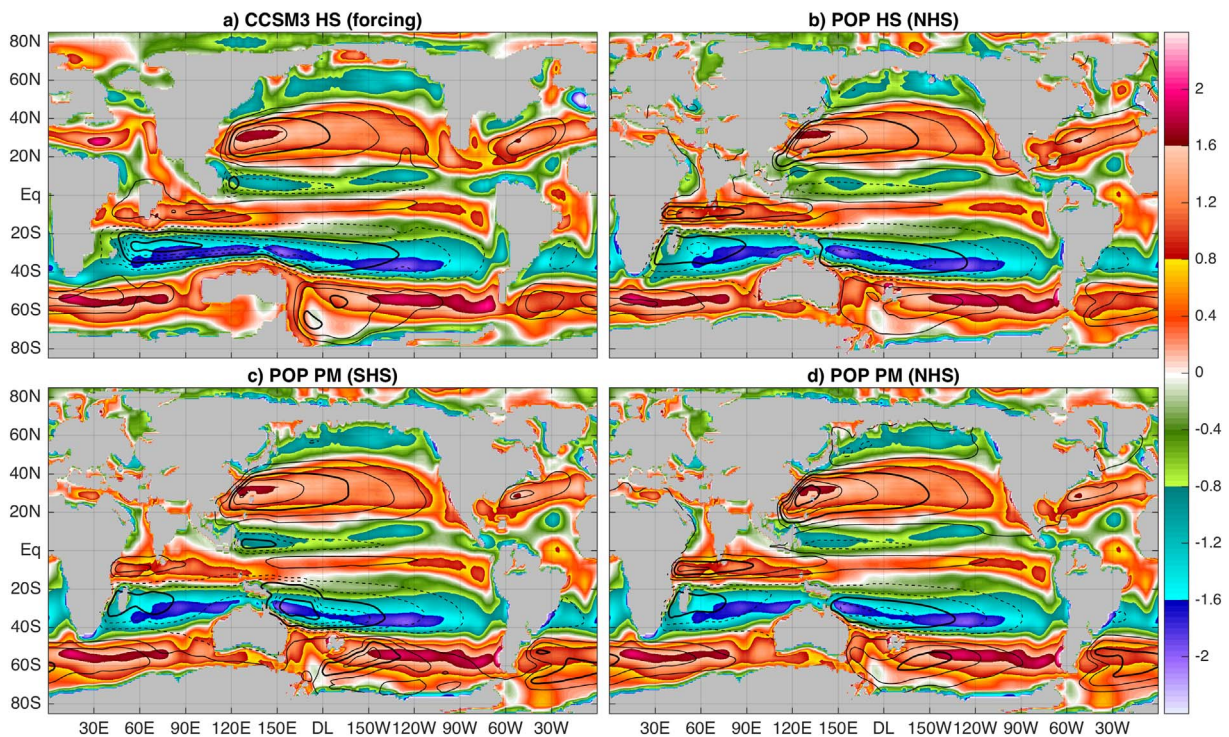

Fig. 9. a) CCSM3 (Eocene forcing) wind stress curl (shading, 10^{-11} Pa/m) and barotropic stream function (contours every 10 Sv, dashed for negative values, thick lines every 30 Sv), and similar for **b)** HS case featuring northern sinking, **c)** PM SHS and **d)** PM NHS cases.
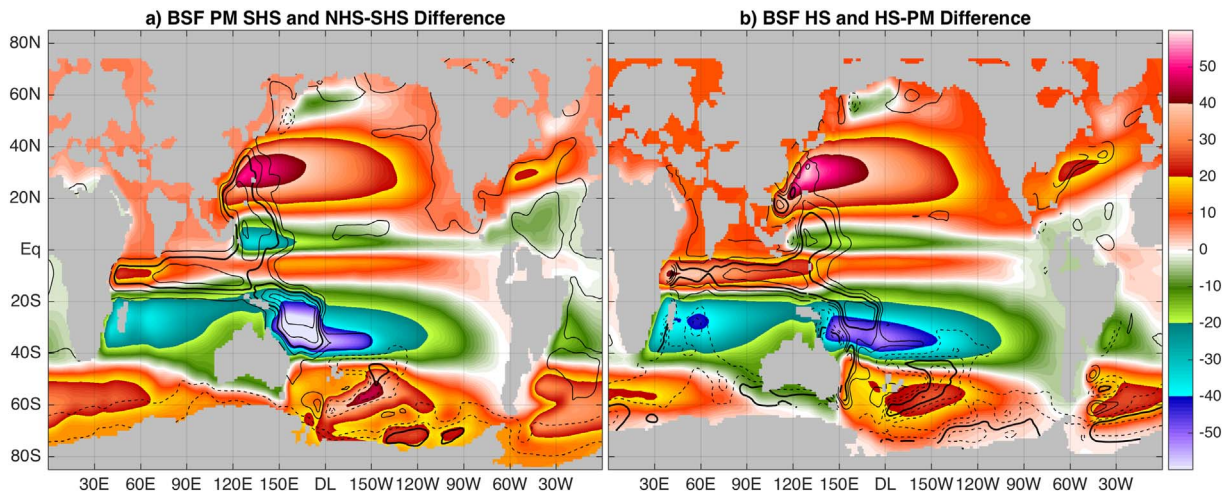
Fig. 10. Barotropic stream function (shading, Sv) and Difference (contours every 5 Sv, dashed for negative values) for **a)** NHS - SHS and **b)** HS - PM cases. The PM case featuring southern sinking is shown in panel a) while the HS case with northern sinking can be seen in panel b) for reference.

overturning states as seen in Fig. 8. In contrast, a global pattern of decreased $\delta^{18}O$ values is caused by higher temperature and salinity of the northerly formed deep water mass. This change is in disagreement with clear increases of benthic oxygen isotope observations across the EOT (Coxall and Wilson, 2011). However, it is possible that the temperature changes shown by the model are not representative as restoring conditions manipulate the properties of surface waters across the source regions. Even prior to the transition, a shift from southern towards northern overturning would have resulted in a reorganisation of the circulation pattern. Associated with such a change would be

cooling of Antarctica and possibly a response in ice growth, stratification and biological activity. Such an event could thus precondition the climate to ice growth when a certain threshold in radiative forcing is reached, or simply change the threshold itself. Most of the considered changes are taking place across the Pacific Ocean, as it is rather weakly stratified across both its northern and southern high latitude regions. The North Atlantic is characterised by weak circulation and ventilation, associated with strong stratification and low surface salinities resulting from a shallow connection to the relatively fresh Arctic Ocean.
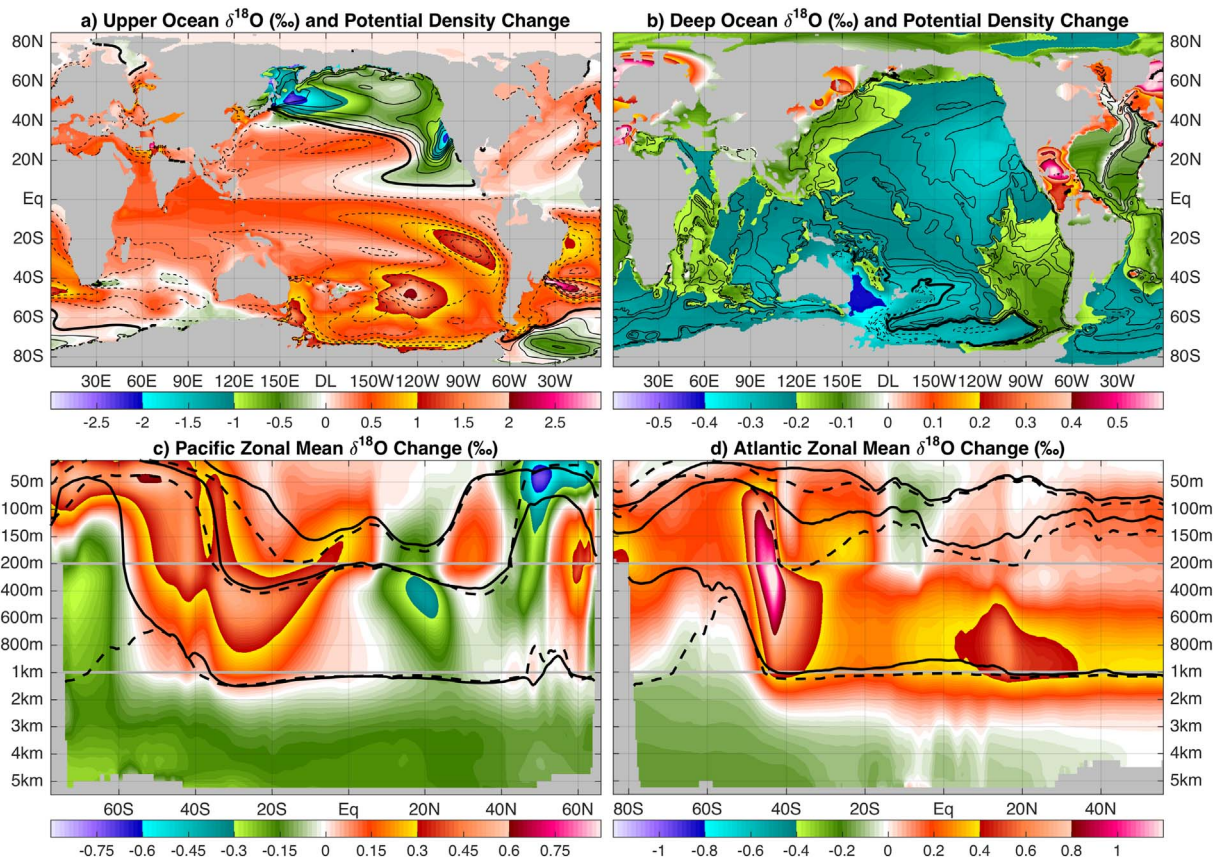

Fig. 11. **a)** Upper (surface to 200 m) and **b)** deep (below 2 km) ocean estimated change in $\delta^{18}O$ isotope values for a NHS-SHS state change (contours: potential density (surface reference) change, solid: positive, dashed: negative). **c)** Zonally averaged Pacific and **d)** Atlantic Ocean cross section of NHS-SHS $\delta^{18}O$ change, contours indicate potential density values at 25, 26 and 27 kg/m^3 for the SHS (solid) and NHS (dashed) situation.

4. Summary and conclusions

Using a global ocean model with two different paleobathymetries for the middle-to-late Eocene (38 Ma), we have shown that the meridional overturning circulation (MOC) is quite sensitive to details in the geometry. In particular, a different choice in reference frame (PaleoMag or HotSpot) can lead to different patterns of the MOC and consequently different sea surface temperature and salinity fields. The underlying reason for this high sensitivity is the existence of two stable equilibria for this Eocene situation under the prescribed forcing as was demonstrated for the PaleoMag configuration (simulations PM and PM Adjusted).

It is often mentioned that multiple equilibria of the meridional overturning circulation (MOC) are an artefact of neglecting the atmospheric feedbacks (and hence would not occur in coupled models), so a discussion is needed here. Indeed, a complete shutdown of the present-day Atlantic MOC has not been found in fully coupled models (Stouffer et al., 2006). However, apart from differences in atmospheric feedbacks between ocean-only and coupled model studies, it is important to distinguish different types of results on multiple equilibria in the relevant modelling literature (mostly for present-day climate studies):

(i) Different statistical equilibria under the same forcing conditions with local differences in deep water formation sites; these equilibria are mostly found only under certain values of parameters (e.g. vertical mixing);

(ii) Different statistical equilibria for the same forcing conditions *and* parameters, showing global changes in observables such as the meridional overturning stream function.

Type (i) multiple equilibria are due to local convective feedbacks, highly sensitive to the surface forcing and basically spurious (Rahmstorf and Willebrand, 1995; den Toom et al., 2011). There are very few results with GCMs on type (ii) multiple equilibria (Hawkins et al., 2011) and such equilibria have not definitely been found yet in coupled models (Stouffer et al., 2006). The reason is not that the multiple equilibria in principle do not exist because of atmospheric feedbacks, but that the computations to systematically find them have not been performed. Moreover, in one present day climate model (FORTE) the existence of mountain ranges seems to influence surface freshwater flux patterns such that the Atlantic MOC is stabilised (Sinha et al., 2012). On the other hand, the analysis of the physics of these equilibria points more and more into the direction that such multiple equilibria do exist in the present-day ocean circulation (Srokosz and Bryden, 2015; Liu et al., 2017). For example, an indicator of the MOC induced Atlantic freshwater export is used as an integral measure of the salt-advection feedback in Huisman et al. (2010).

Our results show type (ii) equilibria in a global ocean model under 38 Ma forcing conditions. To our knowledge this is the first time such multiple equilibria have been found in any global ocean model using a detailed paleobathymetry for the middle-to-late Eocene. It is indeed in an ocean-only context but this is a necessary condition for the existence of these equilibria in the climate system. As for the present-day case, these equilibria can still be relevant in the coupled system and may eventually exist in a fully coupled climate model.

The difference in ocean heat transport between the two equilibria (NHS and SHS) in our results points towards a major redistribution of heat between Northern and Southern hemisphere and is not unusual in ocean-only model studies (e.g. Viebahn et al. (2016)). In coupled models the effect of a MOC switch can be less dramatic in the ocean heat transport, however, the resulting change in surface temperature is often very similar due to other processes such as the atmospheric circulation or sea ice feedbacks (England et al., 2017).

The implied $\delta^{18}O$ changes, based on a very simplified parameterization, due to a shift from SHS to NHS do not agree with the changes seen at the Eocene-Oligocene Transition (EOT). Such a switch in overturning regime would result in significant changes in heat distribution, a possible cooling of Antarctica and large changes in biological activity. Hence, this does not support the idea that a switch in the ocean circulation from SHS to NHS was a first step of the EOT as suggested by Tigchelaar et al. (2011). Nevertheless, such a switch in overturning regime, induced by the changing continental configuration, could have made the climate more susceptible to Antarctic glaciation.

To conclude, multiple equilibria of the meridional overturning circulation may have existed in the middle-late Eocene, but also during other periods through the Cenozoic. As a result, long term shifts between different overturning regimes may be an important contributor to changes in global climate, biology and variability in the Cenozoic and require further study.

References

Baatsen, M., van Hinsbergen, D.J.J., von der Heydt, A.S., Dijkstra, H.A., Sluijs, A., Abels, H.A., Bijl, P.K., 2016. Reconstructing geographical boundary conditions for palaeoclimate modelling during the cenozoic. Clim. Past 12, 1635–1644. http://dx.doi.org/10.5194/cp-12-1635-2016.

Broecker, W.S., 1989. The salinity contrast between the Atlantic and Pacific oceans during glacial time. Palaeoceanography 4 (2), 207–212. http://dx.doi.org/10.1029/PA004i002p00207.

Coxall, H.K., Wilson, P.A., 2011. Early oligocene glaciation and productivity in the eastern equatorial pacific: insights into global carbon cycling. Palaeoceanography 26, PA2221. http://dx.doi.org/10.1029/2010PA002021.

Coxall, H.K., Wilson, P.A., Pälike, H., Lear, C.H., Backman, J., 2005. Rapid stepwise onset of Antarctic glaciation and deeper calcite compensation in the Pacific Ocean. Nature 433, 53–57.

Cramer, B.S., Toggweiler, J.R., Wright, J.D., Katz, M.E., Miller, K.G., 2009. Ocean overturning since the late cretaceous: inferences from a new benthic foraminiferal isotope compilation. Paleoceanography 24, PA4216. http://dx.doi.org/10.1029/2008PA001683.

den Toom, M., Dijkstra, H.A., Wubs, F.W., 2011. Spurious multiple equilibria introduced by convective adjustment. Ocean Model. 38, 126–137. http://dx.doi.org/10.1016/j.ocemod.2011.02.009.

Dupont-Nivet, G., Dai, S., Fang, X., Krijgsman, W., Erens, V., Reitsma, M., Langereis, C., 2008. Timing and distribution of tectonic rotations in the northeastern Tibetan plateau. Geol. Soc. Am. Spec. Pap. 444, 73–87. http://dx.doi.org/10.1130/2008.2444(05).

England, M.H., Hutchinson, D.K., Santoso, A., Sijp, W.P., 2017. Ice-atmosphere feedbacks dominate the response of the climate system to drake passage closure. J. Climate. http://dx.doi.org/10.1175/JCLI-D-15-0554.1.

Gasson, E., Lunt, D.J., DeConto, R., Goldner, A., Heinemann, M., Huber, M., LeGrande, A.N., Pollard, D., Sagoo, N., Sidall, M., Winguth, A., Valdes, P., 2014. Uncertainties in the modelled CO2 threshold for antarctic glaciation. Clim. Past 10, 451–466. http://dx.doi.org/10.5194/cp-10-451-2014.

Gent, P.R., Mcwilliams, J.C., 1990. Isopycnal mixing in ocean circulation. Models. J. Phys. Oceanogr 20, 150–155. http://dx.doi.org/10.1175/1520-0485(1990)020<0150:IMIOCM>2.0.CO;2.

Harzhauser, M., Kroh, A., Mandic, O., Piller, W.E., Göhlich, U., Reuter, M., Berning, B., 2007. Biogeographic responses to geodynamics: a key study all around the oligo-miocene tethyan seaway. Zool. Anz. 246, 241–256. http://dx.doi.org/10.1016/j.jcz.2007.05.001.

Haug, G.H., Tiedemann, R., 1998. Effect of the formation of the Isthmus of Panama on the Atlantic Ocean thermohaline circulation. Nature 393, 673–676.

Hawkins, E., Smith, R.S., Allison, L.C., Gregory, J.M., Woollings, T.J., Pohlmann, H., de Cuevas, B., 2011. Bistability of the atlantic overturning circulation in a global climate model and links to ocean freshwater transport. Geophys. Res. Lett. 38, L10605. http://dx.doi.org/10.1029/2011GL047208.

Haywood, A.M., Dowsett, H.J., Robinson, M.M., Stoll, D.K., Dolan, A.M., Lunt, D.J., Otto-Bliesner, B., Chandler, M.A., 2011. Pliocene model intercomparison project (plioMIP): experimental design and boundary conditions (Experiment 2). Geosci. Model Dev. 4 (3), 571–577. http://dx.doi.org/10.5194/gmd-4-571-2011.

Herold, N., Buzan, J., Seton, M., Goldner, A., Green, J.A.M., Müller, R.D., Markwick, P., Huber, M., 2014. A suite of early Eocene (~ 55 ma) climate model boundary conditions. Geosci. Model Dev. 7 (5), 2077–2090. http://dx.doi.org/10.5194/gmd-7-2077-2014.

Huber, M., Caballero, R., 2011. The early Eocene equable climate problem revisited. Clim. Past 7, 603–633. http://dx.doi.org/10.5194/cp-7-603-2011.

Huisman, S.E., den Toom, M., Dijkstra, H.A., Drijfhout, S., 2010. An indicator of the multiple equilibria regime of the Atlantic meridional overturning circulation. J. Phys. Oceanogr. 40, 551–567. http://dx.doi.org/10.1175/2009JPO4215.1.

Kennett, J.P., 1977. Cenozoic evolution of Antarctic glaciation, the circum-Antarctic current and their impact on global paleoceanography. J. Geophys. Res. 82, 3843–3860.

Large, W.G., McWilliams, J.C., Doney, S.C., 1994. Oceanic vertical mixing: a review and a model with a nonlocal boundary layer parameterization. Rev. Geophys. 32, 363–403. http://dx.doi.org/10.1029/94RG01872.

Liu, W., Xie, S.P., Liu, Z., Liu, J., 2017. Overlooked possibility of a collapsed atlantic meridional overturning circulation in warming climate. Sci. Adv 3, e1601666.

Lunt, D.J., Farnsworth, A., Loptson, C., Foster, G.L., Markwick, P., O'Brien, C.L., Pancost, R.D., Robinson, S.A., Wrobel, N., 2016. Palaeogeographic controls on climate and proxy interpretation. Clim. Past 12 (5), 1181–1198. http://dx.doi.org/10.1007/s10652-009-9154-3.

Müller, R.D., Sdrolias, M., Gaina, C., Roest, W.R., 2008. Age, spreading rates, and spreading asymmetry of the world's ocean crust. Geochem. Geophys. Geosyst. 9 (4). http://dx.doi.org/10.1029/2007GC001743.

Rahmstorf, S., Willebrand, J., 1995. The role of temperature feedback in stabilizing the thermohaline circulation. J. Phys. Oceanogr 25, 787–805. http://dx.doi.org/10.1175/1520-0485(1995)025<0787%3ATROTFI>2.0.CO%3B2.

Seton, M., Müller, R.D., Zahirovic, S., Gaina, C., Torsvik, T., Shephard, G., Talsma, A., Gurnis, M., Turner, M., Maus, S., Chandler, M., 2012. Global continental and ocean basin reconstructions since 200 Ma. Earth Sci. Rev. 113, 212–270. http://dx.doi.org/10.1016/j.earscirev.2012.03.002.

Sinha, B., Blaker, A.T., Hirschi, J.J.M., Bonham, S., Brand, M., Josey, S., Smith, R.S., Marotzke, J., 2012. Mountain ranges favour vigorous atlantic meridional overturning. Geophys. Res. Lett. 39, L02705. http://dx.doi.org/10.1029/2011GL050485.

Smith, R., Jones, P., Briegleb, B., Bryan, F., Danabasoglu, G., Dennis, J., Dukowicz, J., 2010. The parallel ocean program (POP) reference manual. In: Los Alamos National Lab Technical Report, 141.

Smith, R.D., Mcwilliams, J.C., 2003. Anisotropic horizontal viscosity for ocean models.

Ocean Model. 5, 129–156. http://dx.doi.org/10.1016/S1463-5003(02)00016-1.

Srokosz, M.A., Bryden, H.L., 2015. Observing the atlantic meridional overturning circulation yields a decade od inevitable surprises. Science 348 (6241). http://dx.doi.org/10.1126/science.1255575.

Stouffer, R.J., Yin, J., Gregory, J.M., Dixon, K.W., Spelman, M.J., Hurlin, W., Weaver, A.J., Eby, M., Flato, G.M., Hasumi, H., Hu, A., Jungclaus, J.H., Kamenkovich, I.V., Levermann, A., Montoya, M., Murakami, S., Nawrath, S., Oka, A., Peltier, W.R., Robitaille, D.Y., Sokolov, A., Vettoretti, G., Weber, S.L., 2006. Investigating the cause of the response of the thermohaline circulation to past and future climage changes. J. Climate 19, 1365–1387. http://dx.doi.org/10.1175/JCLI3689.1.

Tigchelaar, M., von der Heydt, A.S., Dijkstra, H.A., 2011. A new mechanism for the two-step δ^{18}o signal at the Eocene-Oligocene boundary. Clim. Past 7, 235–247. http://dx.doi.org/10.5194/cp-7-235-2011.

Torsvik, T.H., Van der Voo, R., Preeden, U., Niocaill, C.M.a.c., Steinberger, B., Doubrovine, P.V., van Hinsbergen, D.J.J., Domeier, M., Gaina, C., Tohver, E., Meert, J.G., McCausland, P.J.A., Robin, L., Cocks, M., 2012. Phanerozoic polar wander, paleogeography and dynamics. Earth Sci. Rev. 114, 325–368. http://dx.doi.org/10.1016/j.earscirev.2012.06.007.

van Hinsbergen, D.J.J., de Groot, L.V., van Schaik, S.J., Spakman, W., Bijl, P.K., Sluijs, A., Langereis, C.G., Brinkhuis, H., 2015. A paleolatitude calculator for paleoclimate studies. PloS One 10 (6). http://dx.doi.org/10.1371/journal.pone.0126946. E0126, 946.

Viebahn, J.P., von der Heydt, A.S., LeBars, D., Dijkstra, H.A., 2016. Effects of drake passage on a strongly eddying global ocean. Paleoceanography 31, 564–581. http://dx.doi.org/10.1002/2015PA002888.

von der Heydt, A., Dijkstra, H.A., 2006. Effect of ocean gateways on the global ocean circulation in the late Oligocene and early Miocene. Paleoceanography 21, PA1011. http://dx.doi.org/10.1029/2005PA001149.

Wilson, D.S., Jamieson, S.S.R., Barett, P.J., Leitchenkov, G., Gohl, K., Larter, D., 2012. Antarctic topography at the eocene-oligocene boundary. Palaeogeography, Palaeoclimatology, Palaeoecology 335-336, 24–34. http://dx.doi.org/10.1016/j.palaeo.2011.05.028.

Zachos, J.C., Pagani, M., Sloan, L., Thomas, E., Billups, K., 2001a. Trends, rythms, and aberrations in global climate 65 Ma to present. Science 292, 686–693.